# On Demand Triggering of Edge Localized Instabilities Using External Nonaxisymmetric Magnetic Perturbations in Toroidal Plasmas

J. M. Canik,[1] R. Maingi,[1] T. E. Evans,[2] R. E. Bell,[3] S. P. Gerhardt,[3] B. P. LeBlanc,[3] J. Manickam,[3] J. E. Menard,[3] T. H. Osborne,[2] J.-K. Park,[3] S. F. Paul,[3] P. B. Snyder,[2] S. A. Sabbagh,[4] H. W. Kugel,[3] E. A. Unterberg,[5] and the NSTX Team

[1]*Oak Ridge National Laboratory, Oak Ridge, Tennessee, USA*
[2]*General Atomics, San Diego, California, USA*
[3]*Princeton Plasma Physics Laboratory, Princeton, New Jersey, USA*
[4]*Columbia University, New York, New York, USA*
[5]*Oak Ridge Institute for Science and Education, Oak Ridge, Tennessee, USA*

(Received 17 January 2009; published 26 January 2010)

The application of nonaxisymmetric magnetic fields is shown to destabilize edge-localized modes (ELMs) during otherwise ELM-free periods of discharges in the National Spherical Torus Experiment (NSTX). Profile analysis shows the applied fields increased the temperature and pressure gradients, decreasing edge stability. This robust effect was exploited for a new form of ELM control: the triggering of ELMs *at will* in high performance $H$ mode plasmas enabled by lithium conditioning, yielding high time-averaged energy confinement with reduced core impurity density and radiated power.

DOI: 10.1103/PhysRevLett.104.045001 PACS numbers: 52.55.Fa

The most promising operational scenario for producing fusion energy using the tokamak plasma confinement concept is the high confinement ($H$) mode. The $H$ mode is characterized by steep pressure gradients at the plasma periphery, which lead to strong self-driven plasma currents and an instability known as the edge-localized mode (ELM) [1]. ELMs produce periodic expulsions of energy and particles, posing a serious threat to the lifetimes of plasma facing components (PFCs) from melting and sublimation. The size of ELMs must therefore be tightly controlled in future large devices such as the International Thermonuclear Experimental Reactor (ITER), and several candidate methods for achieving this control are being explored in the fusion community. However, the presence of ELMs has the significant benefit of increasing the effective particle and impurity transport, allowing quasistationary plasma conditions to be achieved [2]. In the absence of ELMs, impurity and radiation buildup is often observed, making the ELM-free $H$ mode a transient state unless a mechanism can be found for increasing particle transport (as seen, e.g., in the QH [3], EDA [4], and RMP [5] $H$ modes). For this reason, optimal control of ELMs can be achieved through suppression of naturally occurring ELMs and reintroduction *at will* as needed for impurity control.

One demonstrated method for ELM control is by the intentional application of nonaxisymmetric magnetic perturbations with control coils. In general, these perturbations consist of a combination of resonant components, with local alignment to the equilibrium magnetic field causing formation of magnetic islands [6] and nonresonant components that can still have large effects on the plasma, e.g., by the braking of toroidal rotation [7]. The use of 3D fields with a strong resonant component [resonant magnetic perturbations (RMPs)] has been shown to mitigate or suppress ELMs by increasing transport and thereby reducing the pedestal pressure gradient in the DIII-D [5] and JET [8] tokamaks, and a flexible coil design has commenced to implement this technique on ITER. The extrapolability of this technique to ITER is uncertain, however, as ELM suppression in DIII-D has not been reproduced as of yet in other fusion devices. Here we demonstrate robust ELM control in a new manner: using lithium coatings to suppress ELMs and then using 3D fields to intentionally trigger ELMs *on demand*. We note that while the triggered ELMs are still larger than desirable, the observed trends indicate concrete ways to substantially reduce the triggered ELM size.

In the remainder of this Letter, we (1) document the existence of a field amplitude threshold for ELM destabilization, (2) show the increase in edge Te (Pe) and its gradient due to the 3D fields, and discuss the reduced stability to edge peeling-ballooning stability, and (3) describe the controllable introduction of ELMs into lithium-enhanced ELM-free $H$ modes in the National Spherical Torus Experiment (NSTX [9]) to reduce impurity accumulation. While ELM destabilization was previously seen in the COMPASS-D [10] and JFT-2M [11] tokamaks, the NSTX experiments have demonstrated unprecedented ELM control: one short 3D field pulse triggers one ELM. The achievable ELM frequency appears to be limited only by the field penetration time, raising the prospect for higher frequency, smaller amplitude triggered ELMs with internal control coils. More generally, this technique may be applicable for introduction of controlled ELMs into ELM-free $H$ modes and perhaps even $VH$ mode [12] in higher aspect ratio tokamaks.

The destabilization of ELMs using nonaxisymmetric perturbations was first observed in NSTX during experiments designed to test ELM suppression using

 

intermediate-$n$ RMPs, as was achieved in DIII-D [5]. In our experiments, the toroidal magnetic field ($B_t$) and plasma current ($I_p$) were fixed at 0.45 T and 800 kA, respectively, and the plasma was heated with up to 6 MW of neutral beam injection ($P_{\mathrm{NBI}}$). The 3D perturbation fields were generated by a set of six midplane coils typically used for error field correction and resistive wall mode (RWM) feedback control [13]. These "RWM coils" are external but close fitting to the vacuum vessel. In the ELM-destabilization experiments, they were configured to apply an $n = 3$ field. The poloidal spectrum of the magnetic perturbation is broad at the plasma edge, extending to mode numbers resonant with the high values of edge safety factor ($q_{95} \sim 10$) used throughout these experiments. The magnitude of the resonant components can be quantified using the Chirikov parameter [14] $\sigma_{\mathrm{ch}}$, which is a measure of island overlap ($\sigma_{\mathrm{ch}} > 1$ indicates a high degree of island overlap and stochasticity). Experiments in DIII-D [15] have shown that ELM suppression is observed when the highly stochastic region with $\sigma_{\mathrm{ch}} > 1$ extends in to normalized poloidal flux $\psi_N = 0.85$. From vacuum field calculations for our experiments, the Chirikov parameter is above unity outside of $\psi_N \sim 0.6$ with 1.1 kA in the midplane coils [16]. However, calculations with the IPEC code [17], which include plasma response to the 3D perturbation, predict some field attenuation, with $\sigma_{\mathrm{ch}} > 1$ only outside of $\psi_N \sim 0.9$ (note that the Chirikov parameter here is only a measure of the resonant field strength; in the ideal model, field lines form closed surfaces, with a nonaxisymmetric spatial shift). Thus, the resonant part of the perturbation spectrum may only be significant at the very edge of the plasma, whereas the nonresonant components are large throughout. In our experiments, the relative importance of the resonant and nonresonant fields is inseparable.

The destabilization of ELMs using magnetic perturbations was first studied in discharges without lithium wall coatings. Those plasmas had double null divertor boundary shapes with $\delta_r{}^{\mathrm{sep}} \sim 0$ ($\delta_r{}^{\mathrm{sep}}$ is the radial distance between the upper and lower divertor separatrices, measured at the outboard midplane), moderate elongation of $\kappa = 2.0$ and high average triangularity $\delta = 0.7$, and $P_{\mathrm{NBI}} = 6$ MW. Under these conditions, the discharges exhibited a relatively long period free of large ELMs (very small Type V ELMs [18] are prevalent in discharges without lithium conditioning), lasting until from just after the $L$-$H$ transition at $t = 0.15$ s to $t \sim 0.5$ s, as shown in Fig. 1(a). The other panels in Fig. 1 demonstrate that, for these plasma conditions, ELMs were triggered within 50 ms of 3D field application, largely independent of the 3D field timing relative to the $L$-$H$ transition. In addition to triggering ELMs, the application of these large 3D fields tended to strongly brake the plasma toroidal rotation and degrade magnetohyrodynamic (MHD) stability [13], so that global instabilities arose shortly after the 3D field was applied, e.g., the long-lived bursts of $D_\alpha$ light after the first few

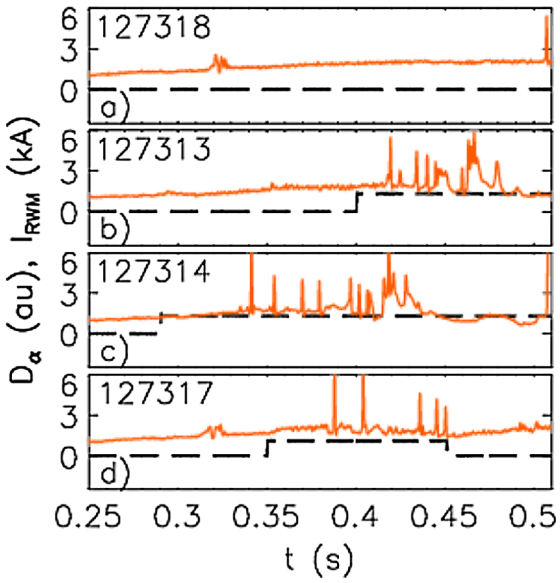


FIG. 1 (color online). $D_\alpha$ emission (solid line) and current in the RWM coils (dashed line) from discharges with (a) no $n = 3$ field and (b)–(d) varying time of $n = 3$ field application.

ELMs in Figs. 1(b) and 1(c). These global instabilities were avoided in other discharges by restricting the perturbation duration, as in Fig. 1(d). When the $n = 3$ field was turned off, the large ELMs ceased [Fig. 1(d)], indicating a direct correlation between ELM stability and the presence of the field.

The ELM-destabilization threshold field strength was identified to be $\Delta B/B_t \sim 6 \times 10^{-3}$ for these discharge conditions, where $\Delta B$ is the total strength of the perturbation at the top of the pedestal (950 A RWM coil current). The 3D fields did not affect ELM stability at $\Delta B/B \sim 5.5 \times 10^{-3}$ (900 A in coil), while at $\Delta B/B \sim 6.1$ and $6.4 \times 10^{-3}$ (0.95 and 1.0 kA, respectively), just above the destabilization threshold, ELMs were intermittently triggered. At the highest field strength of $\Delta B/B \sim 8.3 \times 10^{-3}$ (1.3 kA), a series of regular ELMs was triggered. The data indicate that the triggered ELM frequency increased with the field strength above the destabilization threshold. We note that larger fields led to global instabilities.

The effect of the $n = 3$ field on the plasma profiles was strongest in the toroidal rotation, which showed a global decrease with the applied perturbation that is qualitatively consistent with increased neoclassical toroidal viscosity [19]. While the core electron density and temperature were unaffected by the 3D field, the pedestal electron temperature showed a modest increase with the applied perturbation (Fig. 2). These profiles were constructed with multiple Thomson scattering time slices mapped from lab space to $\psi_N$ from a reference discharge with no $n = 3$ application (time slices combined over 100 ms from a single discharge) and from discharges after the perturbation was applied but before ELMs had begun (time slices ~20 ms after the 3D field application combined from three discharges). These profiles were fitted with "standard"

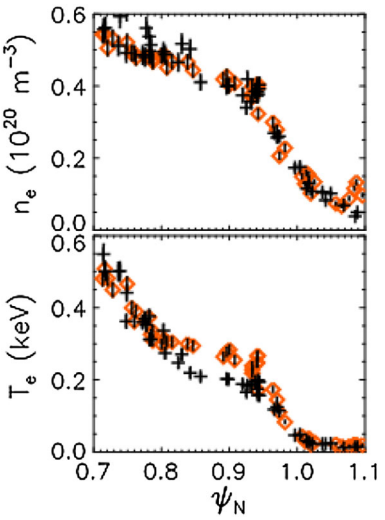


FIG. 2 (color online). Edge profiles of electron (a) density ($n_e$) and (b) temperature ($T_e$) from a discharge with no 3D field applied (black crosses) and at a time after $n = 3$ application but before ELMs (red or gray diamonds).

modified tanh functions [20]; the peak temperature and pressure gradients were ~30% higher with the $n = 3$ field applied. Stability calculations using the PEST ideal MHD code [21] with equilibria based on the experimental pressure profiles indicate the plasmas were unstable to low-$n$ ($n = 2$, 3) peeling-ballooning modes when $n = 3$ was applied, with growth rates of ~1% of the Alfvén frequency. Without the $n = 3$ field, the plasma was calculated to be stable. Although these relatively low growth rate modes may be stabilized by diamagnetic effects [22], the calculations indicate an evolution towards instability after the perturbation is applied. Kinetic profiles nearer to the time of the first ELM will be obtained in upcoming experiments to determine if the edge stability calculations reproduce the instability following the application of the $n = 3$ field.

These results are in apparent contrast to certain experiments at DIII-D where RMPs are used to suppress ELMs in plasmas with ITER-similar shape and collisionality ($\nu^* = q_{95} R \varepsilon^{-3/2} / \lambda_e \leq 0.2$, where $q_{95}$ is the safety factor at the $\psi_N = 0.95$ surface, $R$ is the major radius, $\varepsilon = a/R$ is the inverse aspect ratio, and $\lambda_e$ is the electron mean free path) [23]. The dominant effect of the RMP on the plasma profiles in this case is a significant reduction in density (''density pumpout''), which reduces the peak pedestal pressure gradient sufficiently to stabilize ELMs, consistent with stability calculations with the ELITE code [24]. Neither density pumpout nor ELM suppression has been observed in NSTX. However, at high pedestal-top collisionality ($\nu^* \sim 1$), the impact of the RMP on the plasma profiles in DIII-D is very similar to those seen in NSTX (where $\nu^* \sim 2$): the density is essentially unchanged, toroidal rotation slows, and the electron pedestal pressure is modestly increased [25]. Additionally, experiments at DIII-D using a single row of midplane coils (as opposed to the off-midplane coils typically used for RMP ELM suppression [23]), which produce large nonresonant spectral terms similar to the NSTX coils, have not suppressed ELMs or produced density pumpout [26]. Thus, the NSTX results are reasonably consistent with DIII-D data when the collisionality and perturbation spectra are taken into account. While the observed triggering of ELMs in NSTX remains a clear difference between the machines, the ELM behavior in both devices confirms expectations from peeling-ballooning calculations, i.e., increased (reduced) pressure gradients lead to degraded (improved) edge stability. The remaining mystery is why pedestal transport is affected so differently by the 3D fields in the two machines, with decreased (increased) transport in NSTX (DIII-D).

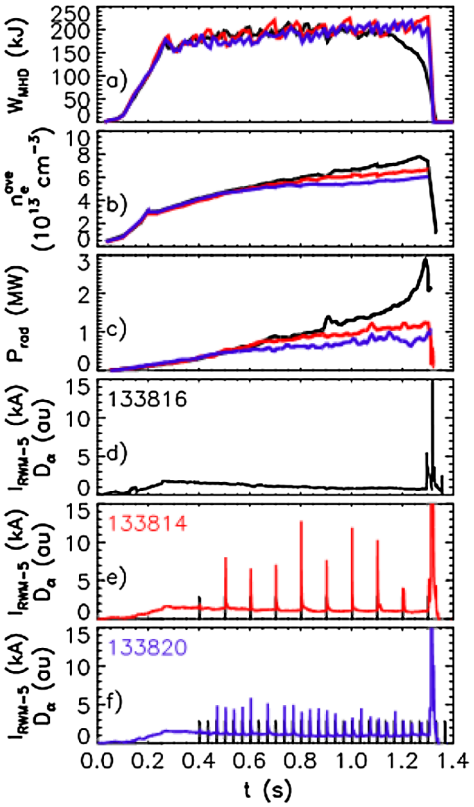


FIG. 3 (color online). Comparison of discharges with lithium conditioning only (black line) and with combined lithium and 3D field-induced ELMs (red and blue or gray lines): (a) stored energy $W_{MHD}$, (b) line-averaged density from Thomson scattering $n_e^{ave}$, (c) total radiated power $P_{rad}$, and (d)–(f) RWM coil current $I_{RWM-5}$ and $D_\alpha$ emission.

Recently, it was demonstrated on NSTX that lithium conditioning of the PFCs improves plasma performance, increasing energy confinement [27], and completely suppressing ELMs [28,29], e.g., as shown by the black curves in Fig. 3. This discharge had $I_p = 800$ kA, $B_t = 0.45$ T, $P_{NBI} = 4$ MW, $\kappa = 2.4$, and $\delta_r^{sep} \sim 0$. Note that the $P_{NBI}$ was reduced compared to the prelithium discharges to avoid reaching the global beta limit. These plasmas also exhibited the nonstationary nature typical of the ELM-free $H$ mode: the particle transport was in effect too low, so that

the density and impurity content increased throughout the discharge, eventually leading to a radiative collapse (Fig. 3).

To reduce the density and impurity accumulation, ELM triggering with 3D fields was added into ELM-free discharges with lithium wall conditioning. Figure 3 shows the time traces from two discharges in which the 3D field was applied in the form of a pulse train, where each pulse has an amplitude of 2.7 kA coil current and a duration of 4 ms. This waveform was chosen to minimize the ''on'' duty cycle of the 3D applied field to reduce the time-averaged impact on plasma rotation and global stability. Two frequencies of the perturbation pulses are shown: 10 and 30 Hz. As shown in the $D_\alpha$ traces in Figs. 3(e) and 3(f), these discharges exhibit ELMs that track the timing and frequency of the 3D field pulses. The density and radiated power evolution were similar between these three discharges before the 3D fields were applied. Once the ELMs began, however, the density and radiated power ramp rates were reduced [Figs. 3(b) and 3(c)]. Near the end of the discharge at $t = 1.3$ s, the density was reduced by 20% and the radiated power by nearly a factor of 3 with 30 Hz ELM triggering relative to the control discharge. The stored energy, on the other hand, was not strongly affected in a time-averaged sense (the ELMs did lead to a transient energy loss) and in fact was sustained for a longer period in the discharge with 3D field pulses. These results demonstrate the deliberate control of the ELM frequency, improving all aspects of the discharge.

These experiments demonstrate the proof of principle of a new high performance discharge scenario: (1) lithium wall coatings to improve particle and energy confinement, and (2) 3D fields to trigger ELMs and reduce particle and impurity confinement. Optimization of the technique is needed to fully arrest the temporal increase of density and radiation, and also to reduce the ELM size; the ELMs that are destabilized by the 3D field with lithium conditioned PFCs tend to be large, with per ELM energy losses of up to 25% of the total stored plasma energy. Fortunately, a dependence on the triggered ELM size on elongation has been observed, which may provide a path for this optimization. Further optimization may also be possible by improving the efficiency with which the 3D fields trigger ELMs. It was observed that the triggered ELM size increased with the period between triggered ELMs, and the likelihood of very large ELMs ($>10\%$) increased substantially for inter-ELM periods $>50$ ms. These long inter-ELM periods were often due to the failure of a 3D field pulse to trigger an ELM, illustrating the importance in increasing not only the ELM frequency but also the triggering reliability to minimize ELM size. The ELM-triggering frequency is presently limited by the $\sim$4 ms field penetration time through the vessel.

In summary, the application of 3D magnetic fields has been observed to destabilize ELMs during periods otherwise free of large ELMs, with a minimum $\Delta B/B$ threshold for destabilization. The triggering effect of the 3D fields has been used to controllably reintroduce ELMs into lithium-enhanced ELM-free $H$ modes; this first proof-of-principle demonstration has been successful in reducing the secular increase of both the plasma density and radiated power. Moreover, high time-averaged energy confinement was maintained while reducing particle confinement. Although further optimization is needed to reduce the triggered ELM size and achieve fully stationary conditions, these results demonstrate the feasibility of an operational scenario wherein lithium wall conditioning is used to improve energy confinement, and ELM pacemaking with nonaxisymmetric magnetic fields is employed for density and impurity control.

This research was supported by the U.S. Department of Energy Contracts No. DE-AC05-00OR22725, No. DE-AC02-09CH11466, No. DE-FC02-04ER54698, and No. DE-FG02-99ER54524.

[1] H. Zohm, Plasma Phys. Controlled Fusion **38**, 105 (1996).
[2] D. N. Hill, J. Nucl. Mater. **241–243**, 182 (1997).
[3] K. H. Burrell *et al.*, Phys. Plasmas **8**, 2153 (2001).
[4] M. Greenwald *et al.*, Plasma Phys. Controlled Fusion **42**, A263 (2000).
[5] T. E. Evans *et al.*, Phys. Rev. Lett. **92**, 235003 (2004).
[6] R. Fitzpatrick, Phys. Plasmas **5**, 3325 (1998).
[7] K. C. Shaing, Phys. Plasmas **10**, 1443 (2003).
[8] Y. Liang *et al.*, Phys. Rev. Lett. **98**, 265004 (2007).
[9] M. Ono *et al.*, Nucl. Fusion **40**, 557 (2000).
[10] S. J. Fielding *et al.*, Europhys. Conf. Abstr. **25**, 1825 (2001).
[11] T. Shoji *et al.*, J. Nucl. Mater. **196–198**, 296 (1992).
[12] G. Jackson *et al.*, Phys. Rev. Lett. **67**, 3098 (1991).
[13] S. A. Sabbagh *et al.*, Phys. Rev. Lett. **97**, 045004 (2006).
[14] B. V. Chirikov, Phys. Rep. **52**, 263 (1979).
[15] M. E. Fenstermacher *et al.*, Phys. Plasmas **15**, 056122 (2008).
[16] J. M. Canik *et al.*, ''ELM destabilization by externally applied non-axisymmetric magnetic perturbations in NSTX,'' Nucl. Fusion (to be published).
[17] J.-K. Park *et al.*, Phys. Plasmas **14**, 052110 (2007).
[18] R. Maingi *et al.*, Nucl. Fusion **45**, 264 (2005).
[19] W. Zhu *et al.*, Phys. Rev. Lett. **96**, 225002 (2006).
[20] R. J. Groebner and T. H. Osborne, Phys. Plasmas **5**, 1800 (1998).
[21] R. Grimm *et al.*, Methods Comput. Phys. **16**, 253 (1976).
[22] P. B. Snyder *et al.*, Phys. Plasmas **9**, 2037 (2002).
[23] T. E. Evans *et al.*, Nucl. Fusion **48**, 024002 (2008).
[24] T. H. Osborne *et al.*, J. Phys. Conf. Ser. **123**, 012014 (2008).
[25] T. E. Evans *et al.*, Nucl. Fusion **45**, 595 (2005).
[26] M. E. Fenstermacher *et al.*, Nucl. Fusion **48**, 122001 (2008).
[27] H. W. Kugel *et al.*, Phys. Plasmas **15**, 056118 (2008).
[28] D. Mansfield *et al.*, J. Nucl. Mater. **390–391**, 764 (2009).
[29] R. Maingi *et al.*, Phys. Rev. Lett. **103**, 075001 (2009).